2010

Design of Organic Tandem Solar Cells Using PCPDTBT: PC61 BM and P3HT: PC71BM

Gon Namkoong
Old Dominion University, gnamkoon@odu.edu

Patrick Boland
Old Dominion University

Keejoo Lee
Old Dominion University

James Dean
Old Dominion University

Original Publication Citation

Namkoong, G., Boland, P., Lee, K., & Dean, J. (2010). Design of organic tandem solar cells using PCPDTBT: PC 61 BM and P3HT: PC 71 BM. *Journal of Applied Physics, 107*(12), 124515. doi:10.1063/1.3448271

Design of organic tandem solar cells using PCPDTBT:$PC_{61}BM$ and P3HT:$PC_{71}BM$

Gon Namkoong,[1,a)] Patrick Boland,[1] Keejoo Lee,[2] and James Dean[2]
[1]*Department of Electrical and Computer Engineering, Applied Research Center, Old Dominion University, 12050 Jefferson Avenue, Newport News, Virginia 23606, USA*
[2]*Department of Aerospace Engineering, Old Dominion University, 4750 Elkhorn Avenue, Norfolk, Virginia 23529, USA*

(Received 1 April 2010; accepted 13 May 2010; published online 28 June 2010)

We conducted optical and electrical simulations with the goal of determining the optimal design for conjugated polymer-fullerene tandem solar cells using poly[2,6-(4,4-bis-(2-ethylhexyl)-4H-cyclopenta[2,1-*b*;3,4-*b*′]dithiophene)-alt-4,7-(2,1,3-benzothiadiazole)] (PCPDTBT): [6,6]-phenyl C_{61} butyric acid methyl ester ($PC_{61}BM$) as a bottom cell and poly(3-hexylthiophene) (P3HT): [6,6]-phenyl C_{71} butyric acid methyl ester ($PC_{71}BM$) as a top cell. The effects of photon density, absorption, balanced and unbalanced charge carrier transport, and bimolecular recombination in the two subcells were incorporated into the simulations. We found that the maximum energy conversion efficiency (η) is 9% when charge carrier mobilities in both top and bottom cells are balanced. However, the efficiency drops significantly if the carrier mobilities are unbalanced in either the top or bottom cell. In addition, we found that unbalanced carrier mobilities in the top cell require a reduction in the thickness of the bottom cell whereas unbalanced bottom cell mobilities require an increase in the thickness of the bottom cell to compensate for the reduced current. © *2010 American Institute of Physics*. [doi:10.1063/1.3448271]

I. INTRODUCTION

The development of photovoltaics to harness limitless and pollution-free solar energy continues to garner an ever-increasing scientific interest. The need for low-cost, easily-producible, and reliable energy sources has spurred research efforts aimed at addressing the development of organic solar cells. Over the last two decades, comprehensive insights and greater understanding of organic materials[1–3] have enabled the continuing evolution of solar energy conversion technology in organic solar cells. Remarkable improvements in performance have been made with *bulk heterojunction* (BHJ) devices[1–3] where organic polymers and fullerene derivatives are randomly mixed to form nanoscale donor/acceptor interfaces. Organic BHJ solar cells have shown drastically improved energy conversion efficiencies of more than 4%.[4–6] However, the limited absorption profiles of currently available organic materials prevent the attainment of higher efficiencies.[7–9] To overcome this shortcoming, multijunction organic solar cells[7–9] have been investigated as a potential design modification for achieving high-efficiency photovoltaics. These multijunction solar cells are arranged in a "tandem" configuration that offers a number of advantages including increasing open circuit voltage (V_{OC}) and short circuit current density (J_{SC}) when connected in series or parallel,[8,9] respectively. The most common configuration comprises a series connection of two or three subcells where the photogenerated current extracted from the tandem structure is determined by the subcell producing the *lowest* value of photocurrent.[9] The V_{OC} of the tandem cell is approximately the sum of each subcell's V_{OC}.[9] Therefore, ideal tandem solar cells in a series configuration require that each subcell be engineered such that light absorption is accurately controlled to balance photocurrent. Recently, Dennler *et al.*,[10] used optical transfer matrix methods (TMM) (Ref. 11) to predict organic thin film thickness for matched photocurrents between two different heterojunction organic blends: poly(3-hexylthiophene) (P3HT): [6,6]-phenyl $C_{61/71}$ butyric acid methyl ester ($PC_{61/71}BM$), and poly[2,6-(4,4-bis-(2-ethylhexyl)-4H-cyclopenta [2,1-*b*;3,4-*b*′] dithiophene)-alt-4,7-(2,1,3-benzothiadiazole)] (PCPDTBT): [6,6]-phenyl $C_{61/71}$ butyric acid methyl ester ($PC_{61/71}BM$). However, in their simulations the balanced photocurrent is calculated based on an assumption of 100% internal quantum efficiency (IQE) where all absorbed photons in the active layers of each subcell ultimately contribute to photocurrent (J_{ph}). In real organic solar cells, several charge transport properties[12–14] such as exciton generation and dissociation, bimolecular recombination, and unbalanced charge transport inside the active layers must be considered when designing optimal tandem structures since those factors cause current density (J_{SC}) to deviate from photocurrent (J_{ph}) obtained when IQE = 100%. Considering all the factors described above, we carried out electrical simulations as well as optical analysis using an organic drift-diffusion model and the optical TMM model tailored for design analysis of tandem organic structures.

II. METHODOLOGY

A. Optical modeling

A schematic of a tandem device is shown in Fig. 1. In the bottom cell, multiple material layers are stacked sequentially: indium tin oxide (140 nm)/poly(3,4 ethylenedioxythiophene) doped with poly(styrene sulfonate) (PEDOT:PSS) (25 nm)/PCPDTBT:$PC_{61}BM$ (d_{bottom})/TiO_2

a)Electronic mail: gnamkoon@odu.edu.

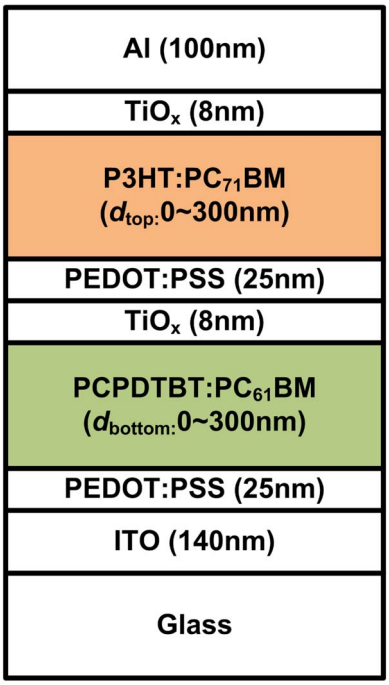

FIG. 1. (Color online) Schematic diagram of a tandem structure used in the simulations. Thicknesses of active layers were varied from 0–300 nm.

(8 nm). The top cell is formed similarly: PEDOT:PSS (25 nm)/P3HT:$PC_{71}BM$ (d_{top})/TiO_2 (8 nm) and finally Al (100 nm) on the top. Note that d_{bottom} and d_{top} are the thicknesses of the active layers allowed to vary up to a maximum of 300 nm. The P3HT polymer is known to have an effective absorption range between UV and 650 nm (Ref. 10) while a low-band gap ($E_g \sim 1.5$ eV) organic material—PCPDTBT—extends the absorption spectra into the infrared region.[5,15,16] Therefore, the combination of these two polymer materials covers a wide spectral absorption range from UV to infrared. It should be noted that this tandem structure has produced energy conversion efficiencies as high as 6.5%.[17]

For the optical analysis of tandem solar cell structures, TMM is performed over a wavelength range from 350–900 nm using standard AM 1.5 sunlight spectra. The optical properties of all the layers are described based on the complex refractive indices, $n' = n(\lambda) + ik(\lambda)$, which are either experimentally obtained from spectroscopic ellipsometry or from the literature.[10] In particular, the refractive index values for P3HT:$PC_{71}BM$ and PCPDTBT:$PC_{61}BM$ are extracted from Ref. 10. For a given set of d_{bottom} and d_{top}, the number of photons (N_{ph}) absorbed in the top and bottom layers are calculated in each subcell as shown in Fig. 2. The absorbed photons are converted to photocurrent by considering charge carrier transport and bimolecular recombination processes and designing an optimal d_{bottom} and d_{top} for each subcell. The maximum thickness considered is around 300 nm due to the fact that both bimolecular recombination and internal resistance of the device significantly increase with excessive thickness and adversely affect energy conversion efficiency.

B. Electrical modeling

The absorbed photons in organic blends generate electron-hole (e-h) pairs or excitons, some of which subsequently dissociate into free-charge carriers at the BHJ interfaces as described by Onsager–Braun theory.[12,13] The transport of dissociated free-charge carriers and Langevin bimolecular recombination[14] are incorporated into a one-dimensional drift-diffusion model and used to estimate the current density and efficiency of organic solar cells. In this model, the mobilities of electron and hole carriers are assumed to be independent of the electric field which is taken to be constant within the organic blends. The net generation rate, $U(x)$, of free-charge carriers can be expressed as[18]

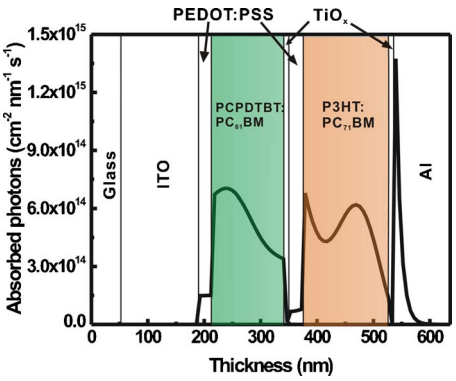

FIG. 2. (Color online) Photon absorption rate profile for a tandem structure composed of active layers of a PCPDTBT:$PC_{61}BM$ bottom cell (130 nm) and a P3HT:$PC_{71}BM$ top cell (150 nm).

$$U(x) = P(x)[G_{e\text{-}h}(x) + R(x)] - R(x), \tag{1}$$

where $P(x)$ is the dissociation probability of bound e-h pairs. $G_{e\text{-}h}(x)$ is the generation rate of photo-induced e-h pairs and $R(x)$ is the Langevin bimolecular recombination rate expressed as

$$R(x) = k_r[n(x)p(x) - n_{int}^2],$$

$$k_r = \frac{q}{\varepsilon}\min(\mu_n, \mu_p). \tag{2}$$

The electron and hole charge carriers are recombined at the rate, k_r, with respect to the intrinsic carrier density n_{int}^2. One should note that k_r is dictated by the mobility of the slower carrier in Eq. (2).

More specifically, the e-h pair dissociation probability at a given pair distance, ξ, is given by

$$p[\xi, F(x), T] = \frac{k_d[\xi, F(x), T]}{k_d[\xi, F(x), T] + k_f(T)}, \tag{3}$$

where k_d is the e-h dissociation rate and k_f is the decay rate to the ground state. The dissociation rate is a function of the e-h pair distance, field strength (F), and temperature (T)

$$k_d[\xi, F(x), T] = \frac{3k_r}{4\pi\xi^3} e^{-E_b/k_BT} \frac{J_1(2\sqrt{-2b})}{\sqrt{-2b}}, \quad b = \frac{q^3F(x)}{8\pi\varepsilon k_B^2T^2}, \tag{4}$$

where E_b is the e-h binding energy and J_1 is the Bessel function of the first kind. In disordered polymer-fullerene systems, the e-h pair distance, ξ, is not constant. Accordingly, the overall dissociation probability of e-h pairs must be treated statistically by integrating the probability function in

TABLE I. Overview of material parameters used in the fit to the experimental data.

		Numerical value		
	Symbol	P3HT:PCBM	PCPDTBT:PCBM	Unit
Effective energy band gap	E_g	1.1	1.0	eV
Dielectric constant	ε	$3.4\varepsilon_0$	$3.4\varepsilon_0$	F/m
Effective density of states	N_{eff}	2.5×10^{19}	2.5×10^{19}	cm^{-3}
e-h pair distance	a	1.12	1.47	nm
Decay rate	k_f	3×10^5	1×10^5	1/s
Electron mobility	μ_e	9×10^{-3}	6×10^{-3}	$\text{cm}^2/\text{V s}$
Hole mobility	μ_h	7×10^{-3}	1×10^{-4}	$\text{cm}^2/\text{V s}$

Eq. (3) over all spatial e-h pair distances $(\xi=0,\infty)$ as

$$P[a,F(x),T]=\int_{\xi=0}^{\xi=\infty} p[\xi,F(x),T]\frac{4\xi^2}{\sqrt{\pi}a^3}e^{-(\xi/a)^2}d\xi, \tag{5}$$

where a Gaussian function normalized to the most probable distance a is used to represent a selected distribution profile.

Using the Poisson equation, potential $\psi(x)$ and electric field are calculated at the position x as

$$\varepsilon\frac{\partial^2\psi(x)}{\partial x^2}=-\varepsilon\frac{\partial F(x)}{\partial x}=q[n(x)-p(x)], \tag{6}$$

where ε is the dielectric constant of organic blend, q is the elementary charge, and $n(x)$ and $p(x)$ are the electron and hole densities, respectively. The current densities in terms of drift-diffusion of the charge carriers are calculated using the continuity equations for the electron $[J_n(x)]$ and hole current densities $[J_P(x)]$

$$q\frac{\partial J_n(x)}{\partial x}+U(x)=0,$$

$$-q\frac{\partial J_p(x)}{\partial x}+U(x)=0,$$

$$J_n(x)=-q\mu_n\left[n(x)\frac{\partial\psi(x)}{\partial x}-V_t\frac{\partial n(x)}{\partial x}\right],$$

$$J_p(x)=-q\mu_p\left[p(x)\frac{\partial\psi(x)}{\partial x}+V_t\frac{\partial p(x)}{\partial x}\right], \tag{7}$$

where μ_n and μ_p are the mobilities of the electrons and holes, respectively, and $V_t=k_BT/q$ is the thermal voltage. The coupled nonlinear equations described above are solved iteratively to obtain the steady state condition for the electric potential, free-charge concentrations, and current densities.

C. Comparison with experimental data

Using the optical and electrical models, material parameters for P3HT:PCBM and PCPDTBT:PCBM were derived and are summarized in Table I. The parameters for P3HT:PCBM were extracted based on device efficiencies over 4% and an active layer thickness of 175 nm.[19] The reference mobility ratio between electrons and holes $(\mu_e:\mu_h)$ is taken close to 1 which is required to achieve higher energy conversion efficiencies in thicker organic blends. Even though these mobilities listed in Table I are one order of magnitude higher than the experimentally measured values from Ref. 19, our values have been fitted to other experimental data[20] where the device thickness exceeded 300 nm as can be seen in Fig. 3(a). In contrast, device parameters for PCPDTBT:PCBM are not well investigated requiring that we use experimental current-voltage (IV) characteristics from Ref. 5. Results are shown in Fig. 3(b). The best fit values for the pair separation distance, $a=1.47$ nm, and decay rate, $k_f=10^5$ 1/s, were determined by comparing experimental IV characteristics with fitting data for an active layer thickness of 110 nm. These values differ somewhat compared to previously reported values[21] where $a=2.1$ nm and the decay

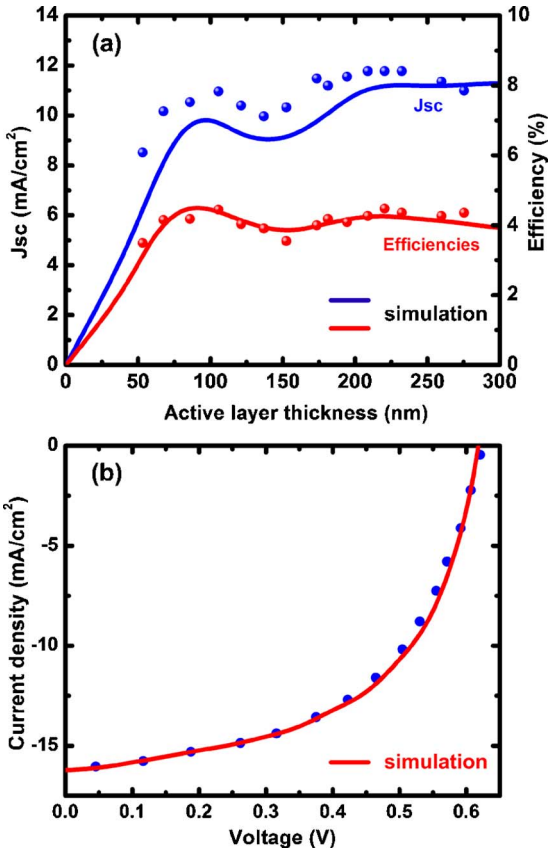

FIG. 3. (Color online) (a) Comparison of current density and efficiencies between experimental data (dots) and simulation (solid lines) of P3HT:PCBM (Ref. 20) and (b) comparison of simulated and experimentally-measured IV characteristics of PCPDTBT:PCBM having an active layer thickness of 110 nm (Ref. 5).

TABLE II. Mobilities of electrons and holes for Cases I, II, and III.

	Numerical value	
	Bottom cell PCPDTBT:$PC_{61}BM$ (cm^2/V s)	Top cell P3HT:$PC_{71}BM$ (cm^2/V s)
Case I	$\mu_e=6\times10^{-3}$	$\mu_e=9\times10^{-3}$
	$\mu_h=1\times10^{-3}$	$\mu_h=7\times10^{-4}$
Case II	$\mu_e=6\times10^{-3}$	$\mu_e=9\times10^{-3}$
	$\mu_h=1\times10^{-3}$	$\mu_h=7\times10^{-3}$
Case III	$\mu_e=6\times10^{-3}$	$\mu_e=9\times10^{-3}$
	$\mu_h=1\times10^{-4}$	$\mu_h=7\times10^{-3}$

rate $k_f=1.7\times10^7$ 1/s. Such a difference might come from the improvement in optical and electrical performance that results from adding alkane dithiols to PCPDTBT polymer-fullerene blends.[5]

III. RESULTS AND DISCUSSION

Current matching between subcells in series tandem structures is a critical performance requirement where the number of absorbed photons,[10] charge carrier transport, and bimolecular recombination[22] must be optimized to balance the photocurrent. Low charge carrier mobilities and unbalanced charge distribution that results from unbalanced electron/hole mobilities in organic photovoltaics[23,24] are characteristics of organic solar cells that make it complicated to match current densities between subcells. In this study, three different cases were investigated employing a PCPDTBT:$PC_{61}BM$ bottom subcell and a P3HT:$PC_{71}BM$ top cell: Case I—unbalanced charge carrier mobilities in the P3HT:$PC_{71}BM$ subcell with balanced mobilities in the PCPDTBT:$PC_{61}BM$ cell, Case II—balanced charge carrier mobilities in both top and bottom subcells, and Case III—unbalanced carrier mobility in PCPDTBT:$PC_{61}BM$ with balanced mobilities in P3HT:$PC_{71}BM$. Table II shows electron and hole mobilities for each subcell in each of the three cases. The values for the electron and hole mobilities for P3HT:PCBM (Ref. 25) and PCPDTBT:PCBM (Ref. 16) are varied based on experimental results reported in the literature. To consider unbalanced charge carrier transport, we set hole mobility one order of magnitude lower than that of the electrons as this is consistent with experimentally observed values for organic blends.[16,25]

Figure 4 shows an isoline graph where the current densities for each case are matched between the top and bottom cells as a function of both cell thicknesses. The J_{SC} values for each case were calculated based on both electrical and optical models described in Sec. II. We first calculated the isoline as a guideline where the total number of photons, N_{ph}, absorbed in each cell are matched and converted into photocurrent density, J_{ph}, by assuming that IQE was equal to 100%. J_{SC} deviated from the J_{ph} isoline in all three Cases, I, II, and III. When charge carriers in both cells are balanced (Case II), J_{SC} is very close to J_{ph}. However, when charge carriers are unbalanced as in Cases I and III, the thickness of each subcell will be modified dependent upon the degree of unbalance of charge carrier mobilities in the bottom or top cell. In Case I where the P3HT:$PC_{71}BM$ top cell has unbalanced

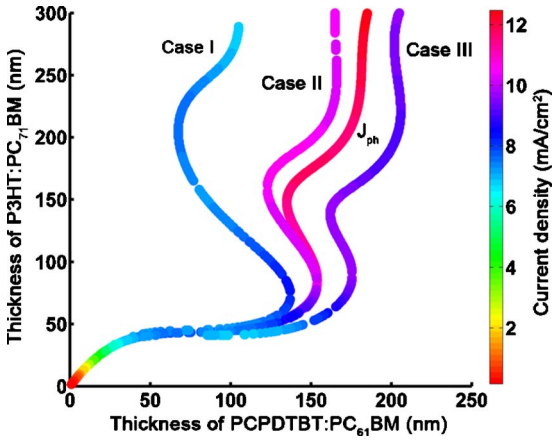

FIG. 4. (Color online) Isolines matching current densities between a PCPDTBT:$PC_{61}BM$ bottom cell and a P3HT:$PC_{71}BM$ top cell for different Cases I, II, and III. As a guide, an isoline of J_{ph} was calculated by assuming that the absolute numbers of photons in each subcell are completely converted to photocurrent (J_{ph}). Current densities in each isoline are indicated by different levels of color.

carrier mobilities, it is observed that d_{bottom} (PCPDTBT:$PC_{61}BM$) should be reduced. In contrast, in Case III where the PCPDTBT:$PC_{61}BM$ bottom cell has unbalanced charge mobilities, d_{bottom} (PCPDTBT:$PC_{61}BM$) should be increased.

To investigate the effect of charge carrier mobility on isoline variations, we calculated the J_{SC} for each cell by fixing d_{top} (P3HT:$PC_{71}BM$)=100 nm while varying d_{bottom} (PCPDTBT:$PC_{61}BM$) from 0 to 300 nm as shown in Fig. 5. Interestingly in Fig. 5(a), J_{ph} for P3HT:$PC_{71}BM$ continuously decreases with increased d_{bottom} while J_{ph} for PCPDTBT:$PC_{61}BM$ continuously increases though at a slower rate from 180 to 300 nm thickness. In this configuration, the J_{ph} in each cell are matched with the active layer thicknesses of $d_{bottom}=150$ nm and $d_{top}=100$ nm as shown in Fig. 5(a). When hole mobility dropped by one order of magnitude from $\mu_h=7\times10^{-3}$ to $\mu_h'=7\times10^{-4}$ cm^2/V s with a constant electron mobility of $\mu_e=9\times10^{-3}$ cm^2/V s in P3HT:$PC_{71}BM$ (Case I), a significant drop in J_{SC} was observed. Therefore, d_{bottom} should be modified to have a thinner active layer. The shift toward a thinner d_{bottom} is required to reduce the absorption of N_{ph} in the bottom cell, thereby reducing J_{SC} in PCPDTBT:$PC_{61}BM$ and subsequently matching the reduced J_{SC} of the top cell. It should be also noted that increasing d_{top} will lead to increased bimolecular recombination and subsequently more current density drops in the top solar cell. This in turn will require d_{bottom} to be made thinner. This can be seen in Fig. 4 where increased deviation from J_{ph} is observed with increased d_{top} which leads to a decrease in the thickness of the active layer, d_{bottom}, in the bottom cell.

In Case III where the charge carrier mobility of PCPDTBT:$PC_{61}BM$ in the bottom cell is unbalanced, the J_{SC} is shifted toward the right away from J_{ph} in Fig. 4 indicating that a thicker active layer in the bottom solar cell is required to match current between the bottom and top solar cells [Fig. 5(b)]. Since the drop in J_{SC} in the bottom cell occurs due to increased bimolecular recombination that results from de-

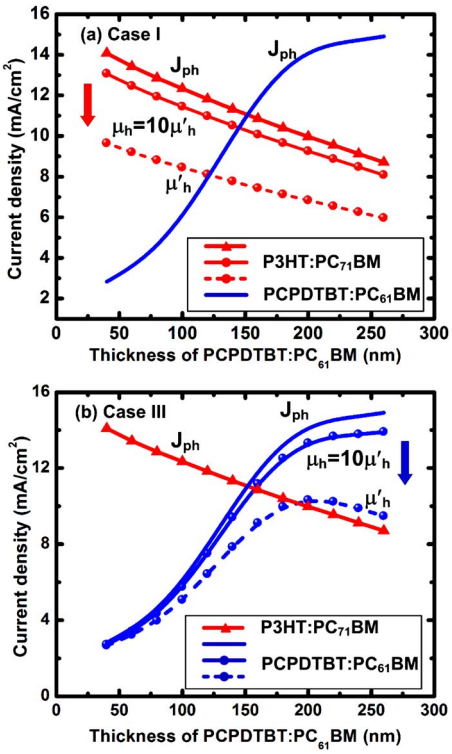

FIG. 5. (Color online) Variation in isolines with different charge carrier mobilities for (a) Case I and (b) Case III as a function of d_{bottom} (PCPDTBT:$PC_{61}BM$) but with fixed $d_{top}=100$ nm (P3HT:$PC_{71}BM$). For Case I, current density (solid line with spheres) slightly deviates from J_{ph} with $\mu_h=7\times10^{-3}$ cm^2/V s and $\mu_e=9\times10^{-3}$ cm^2/V s in P3HT:$PC_{71}BM$. With $\mu'_h=7\times10^{-4}$ cm^2/V s and $\mu_e=9\times10^{-3}$ cm^2/V s, a significant current drop (dotted line with spheres) was observed. For Case III, when the hole mobility in PCPDTBT:$PC_{61}BM$ was dropped from $\mu_h=1\times10^{-3}$ cm^2/V s (blue solid line with spheres) to $\mu'_h=1\times10^{-4}$ cm^2/V s (blue dotted line with spheres) with constant $\mu_e=6\times10^{-3}$ cm^2/V s, a significant current drop was observed. Solid lines indicate the photocurrent J_{ph} generated with IQE=100%.

creasing hole mobility from $\mu_h=1\times10^{-3}$ to $\mu'_h=1\times10^{-4}$ cm^2/V s and holding electron mobility constant at $\mu_e=6\times10^{-3}$ cm/V s, it is necessary to drop J_{SC} in the top cell. This can be achieved by increasing d_{bottom} which will have the effect of allowing more photons to be absorbed in the bottom solar cell. Consequently, N_{ph} in the bottom cell is increased, thereby, decreasing N_{ph} in the top cell and subsequently matching the J_{SC} between top and bottom cells.

To estimate energy conversion efficiency in tandem solar cells, we calculated J_{SC}, fill factor (FF), and V_{OC} using the following relations:

$$V_{tandem} = V_{bottom} + V_{top},$$

$$J_{tandem} = \min(J_{bottom}, J_{top}), \tag{8}$$

The simulated results are shown in Fig. 6. As expected, when charge carriers in both the bottom and top cells are balanced for Case II, the highest J_{SC}, V_{OC}, and energy conversion efficiency are obtained. The J_{SC} initially increases but reaches a plateau of ~11 mA/cm^2 as shown in Fig. 6(a). In contrast, FF in Fig. 6(b) continuously decreases with increased active layer thickness. Therefore, the highest efficiency obtained was about 9% with active layer thicknesses of d_{bottom} (PCPDTBT:$PC_{61}BM$)=146 nm and d_{top} (P3HT:$PC_{71}BM$)=106 nm, as shown in Fig. 6(c). For a wide range of active layer thicknesses for the bottom and top cells for Case II, an overall energy conversion efficiency of 8%–9% can be achieved. However, it should be noted that in our simulations balanced high mobilities in the subcells led to high FF (~0.74) and a corresponding η=9%. If the experimental FF=0.67 is considered,[17] the realistic energy conversion efficiency should reach approximately 8.14%. On the other hand, the energy conversion efficiency for Cases I and III recorded below 6%. For Case I, a rapid drop in current density in Fig. 6(a) is observed and is responsible for the lower η. As shown in Fig. 7(a) for the IV characteristics of individual cells in the tandem structure for Case I, the P3HT:$PC_{71}BM$ top cell has unbalanced charge carrier mobilities that are attributed to the lower current density of the

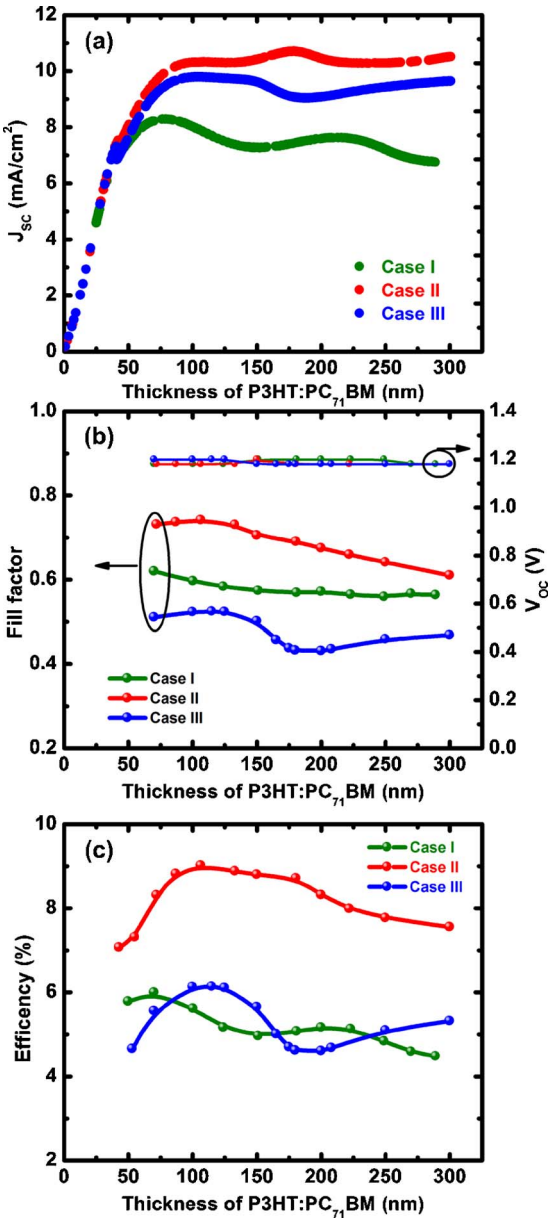

FIG. 6. (Color online) (a) Current density, (b) FF and V_{OC}, and (c) efficiency for tandem solar cells for each of the different Cases I, II, and III as a function of a P3HT:$PC_{71}BM$ thickness. The highest efficiency of 9% in Case II is achieved with active layer thicknesses of d_{bottom} (PCPDTBT:$PC_{61}BM$)=146 nm and d_{top} (P3HT:$PC_{71}BM$)=106 nm.

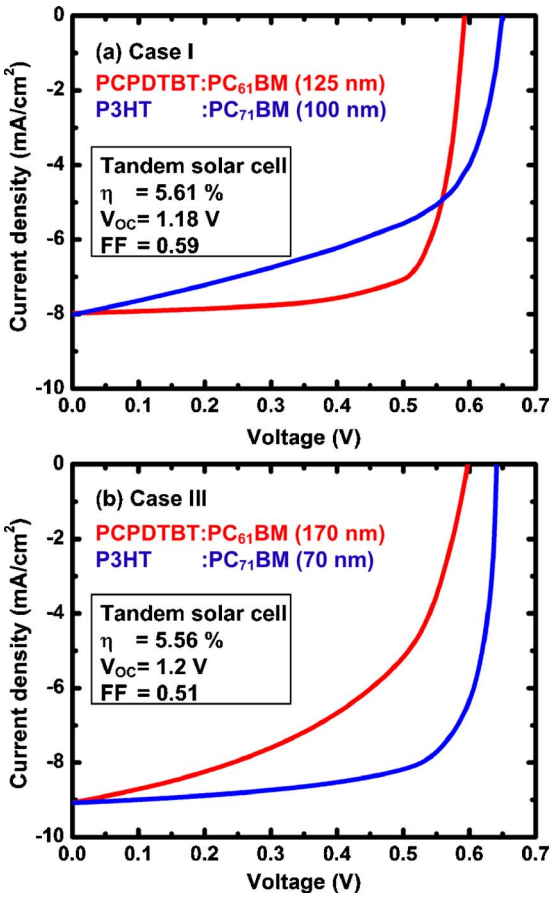

FIG. 7. (Color online) IV characteristics of each subcell in the tandem structures for (a) Case I and (b) Case III with different active layer thicknesses.

tandem solar cell design. In contrast, higher current density is observed for Case III but the FF is governed by the PCPDTBT:PC_{61}BM bottom cell and is much lower than that of Case I as shown in Fig. 7(b). The reported FF for PCPDTBT:PCBM shows values less than 0.55 (Refs. 5, 17, and 26) while P3HT:PCBM produces FF=0.6–0.69.[17,25] Therefore, in Case III the lower FF of the bottom PCPDTBT:PC_{61}BM cell restricts the efficiency.

IV. CONCLUSION

Based on optical and electrical simulations, we investigated the optimal design of tandem organic solar cells using PCPDTBT:PC_{61}BM for the bottom subcell and P3HT:PC_{71}BM for the top cell. It is found that the achievable energy conversion efficiency of this device structure can be as high as 9%. However, if charge carriers are unbalanced in either subcell, energy conversion efficiencies can drop to 4%–6% as a result of either lower current density or lower FF in the subcell. Therefore, it is required that charge carrier mobilities be balanced in each subcell to achieve the highest energy conversion efficiencies in organic tandem structures.

ACKNOWLEDGMENTS

This research was supported by a Multidisciplinary Seed Grant from the Office of Research at Old Dominion University.

[1]G. Yu and A. J. Heeger, J. Appl. Phys. **78**, 4510 (1995).
[2]G. Yu, J. Gao, J. C. Hummelen, F. Wudl, and A. J. Heeger, Science **270**, 1789 (1995).
[3]J. J. M. Halls, C. A. Walsh, N. C. Greenham, E. A. Marseglia, R. H. Friend, S. C. Moratti, and A. B. Holmes, Nature (London) **376**, 498 (1995).
[4]J. Y. Kim, S. H. Kim, H. H. Lee, K. Lee, and A. J. Heeger, Adv. Mater. (Weinheim, Ger.) **18**, 572 (2006).
[5]J. Peet, J. Y. Kim, N. E. Coates, W. L. Ma, D. Moses, A. J. Heeger, and G. C. Bazan, Nature Mater. **6**, 497 (2007).
[6]S. H. Park, A. Roy, S. Beaupre, S. Cho, N. Coates, J. S. Moon, D. Moses, M. Lerclerc, K. Lee, and A. J. Heeger, Nat. Photonics **3**, 297 (2009).
[7]G. Dennler, M. C. Scharber, T. Ameri, P. Denk, K. Forberich, C. Waldauf, and C. J. Brabec, Adv. Mater. (Weinheim, Ger.) **20**, 579 (2008).
[8]A. Hadipour, B. de Boer, and P. W. M. Blom, Adv. Funct. Mater. **18**, 169 (2008).
[9]A. Hadipour, B. de Boer, and P. W. M. Blom, Org. Electron. **9**, 617 (2008).
[10]G. Dennler, K. Forberich, T. Ameri, C. Waldauf, P. Denk, and C. J. Brabec, J. Appl. Phys. **102**, 123109 (2007).
[11]L. A. A. Pettersson, L. S. Roman, and O. Ingana, J. Appl. Phys. **86**, 487 (1999).
[12]L. Onsager, Phys. Rev. **54**, 554 (1938).
[13]C. L. Braun, J. Chem. Phys. **80**, 4157 (1984).
[14]P. Langevin, Ann. Chim. Phys. **28**, 433 (1903).
[15]C. Soci, I. W. Hwang, D. Moses, Z. Zhu, D. Waller, R. Gaudiana, C. J. Brabec, and A. J. Heeger, Adv. Funct. Mater. **17**, 632 (2007).
[16]M. Morana, M. Wegscheider, A. Bonanni, N. Kopidakis, S. Shaheen, M. Scharber, Z. Zhu, D. Waller, R. Gaudiana, and C. Brabec, Adv. Funct. Mater. **18**, 1757 (2008).
[17]J. Y. Kim, K. Lee, N. E. Coates, D. Moses, T.-Q. Nguyen, M. Dante, and A. J. Heeger, Science **317**, 222 (2007).
[18]L. J. A. Koster, E. C. P. Smits, V. D. Mihailetchi, and P. W. M. Blom, Phys. Rev. B **72**, 085205 (2005).
[19]Y. Kim, S. Cook, S. M. Tuladhar, S. A. Choulis, J. Nelson, J. R. Durrant, D. D. C. Bradley, M. Giles, I. McCulloch, C.-S. Ha, and M. Ree, Nature Mater. **5**, 197 (2006).
[20]A. J. Moule and K. Meerholz, Appl. Phys. B: Lasers Opt. **92**, 209 (2008).
[21]M. Lenes, M. Morana, C. J. Barbec, and P. W. M. Blom, Adv. Funct. Mater. **19**, 1106 (2009).
[22]A. Pivrikas, N. S. Sariciftci, G. Juska, and R. Osterbacka, Prog. Photovoltaics **15**, 677 (2007).
[23]M. Lenes, L. J. A. Koster, V. D. Mihailetchi, and P. W. M. Blom, Appl. Phys. Lett. **88**, 243502 (2006).
[24]L. J. A. Koster, V. D. Mihailetchi, and P. W. M. Blom, Appl. Phys. Lett. **88**, 052104 (2006).
[25]V. D. Mihailetchi, H. Xie, B. de Boer, L. J. A. Koster, and P. W. M. Blom, Adv. Funct. Mater. **16**, 699 (2006).
[26]D. Mühlbacher, M. Scharber, M. Morana, Z. Zhu, D. Waller, R. Gaudiana, and C. Brabec, Adv. Mater. (Weinheim, Ger.) **18**, 2884 (2006).